AGU100 ADVANCING EARTH AND SPACE SCIENCE

Geophysical Research Letters

RESEARCH LETTER
10.1029/2018GL078682

Key Points:
- Deep convection is invigorated above a modeled shipping lane in cloud-resolving simulations
- Updraft area and hydrometeor mass are enhanced in the mixed-phase region above the shipping lane
- Cloud radiative effects are intensified; change in net radiative flux at top-of-atmosphere is weak

Correspondence to:
P. N. Blossey,
pblossey@uw.edu

Citation:
Blossey, P. N., Bretherton, C. S., Thornton, J. A., & Virts, K. S. (2018). Locally enhanced aerosols over a shipping lane produce convective invigoration but weak overall indirect effects in cloud-resolving simulations. *Geophysical Research Letters*, *45*, 9305–9313. https://doi.org/10.1029/2018GL078682

Received 8 MAY 2018
Accepted 28 JUL 2018
Accepted article online 6 AUG 2018
Published online 14 SEP 2018

Locally Enhanced Aerosols Over a Shipping Lane Produce Convective Invigoration but Weak Overall Indirect Effects in Cloud-Resolving Simulations

Peter N. Blossey[1], Christopher S. Bretherton[1,2], Joel A. Thornton[1], and Katrina S. Virts[3]

[1]Department of Atmospheric Sciences, University of Washington, Seattle, WA, USA, [2]Department of Applied Mathematics, University of Washington, Seattle, WA, USA, [3]NASA Marshall Space Flight Center, Huntsville, AL, USA

Abstract The effect of aerosol emissions from an active shipping lane in the Indian Ocean is simulated using an idealized framework in a cloud-resolving model. Increased aerosol concentrations over the modeled shipping lane lead to increased cloud droplet number, cloud liquid mass, ice hydrometeor mass, and simulated radar reflectivity. The invigoration of deep convection induces mesoscale uplift and increased precipitation over the shipping lane. A predicted increase in the prevalence of both strong updrafts and radar echoes aloft is suggestive of enhanced lightning activity over the shipping lane, as observed in a recent study. Cloud radiative effects, both shortwave and longwave, are intensified over the shipping lane, but the change in the net radiative flux at top of atmosphere is not significantly different from zero.

Plain Language Summary Clouds are made up in part of droplets that form on small, airborne particles that come from both natural and manmade sources. Rain tends to form more slowly in clouds with more numerous and smaller cloud droplets, so that clouds in polluted regions (with higher particle concentrations) may be slower to rain than similar ones in cleaner regions. Past research has suggested that thunderstorms forming over polluted regions may grow more intense than similar storms that form in cleaner regions, because less cloud water is removed by rain and more of it freezes higher up in the storm. This freezing releases heat that further intensifies the storm. Recently, lightning was found to occur more often above shipping lanes in South and Southeast Asia than away from the shipping lane. We have simulated the approximate effect of ship-derived pollution on the storms and found that storms are strengthened over the shipping lane. Increases in rainfall and cloud cover are modest. However, stronger changes occur higher up in the storms with increases in the occurrence of large ice particles that are also seen by a satellite over the shipping lane in the Indian Ocean.

1. Introduction

Aerosols impact the properties of liquid clouds by providing nuclei onto which water vapor condenses to form cloud droplets. Changing anthropogenic emissions of aerosols affects Earth's energy balance by their direct radiative effects and by modifying the microphysical, macrophysical, and radiative properties of clouds. These aerosol-cloud interactions represent a major component of the uncertainty in the prediction of climate change (Boucher et al., 2013).

Much attention has focused on the interactions of aerosols with shallow maritime clouds due to their high cloud cover and susceptibility to aerosol perturbations, but aerosol can also impact deep convective clouds (Tao et al., 2012), which play a prominent role in the Earth's energy and water cycles. In atmospheric columns with active deep convection, we anticipate that increased aerosol concentrations in the boundary layer lead to higher cloud droplet number concentrations and smaller cloud drops in the liquid clouds at low levels. This slows the formation of rain by collision and coalescence and may allow greater amounts of liquid water to be carried up above the freezing level. The freezing of this additional liquid (via accretion onto ice hydrometeors or droplet freezing) would release additional latent heat and increase the buoyancy of these deep convective updrafts. This source of additional heating and buoyancy has been hypothesized to invigorate deep convection, producing stronger updrafts and more anvil cirrus (Rosenfeld et al., 2008). Recently, Fan et al. (2018) proposed a second mechanism for aerosol invigoration of deep convection: Strong convective updrafts in polluted regions could experience additional latent heating because the activation of ultrafine aerosol particles

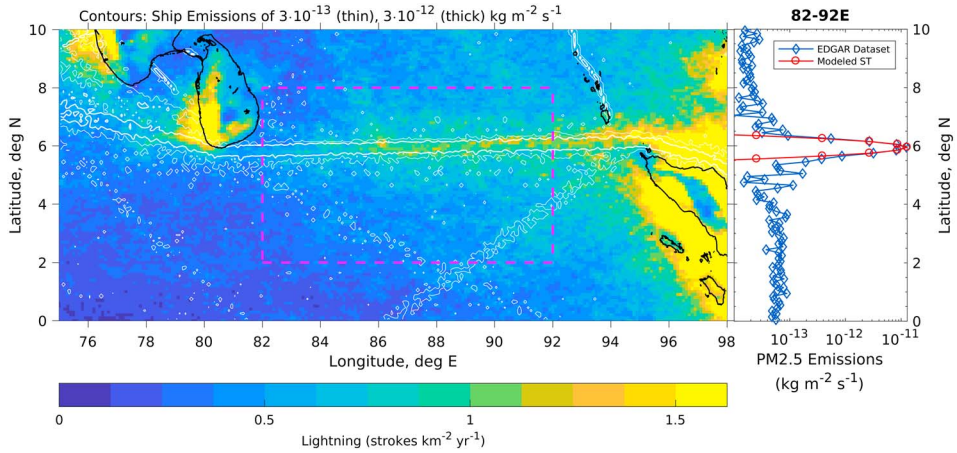

Figure 1. (a) Annual average lightning flash rate from Worldwide Lightning Location Network (color) and shipping emissions from the EDGAR database (white contours). (b) Zonally averaged shipping emissions (blue) and a Gaussian approximation of emissions enhancement over the shipping lane (red). (a) is adapted from Figure 1 of Thornton et al. (2017), which describes the data in detail. EDGAR = Emissions Database for Global Atmospheric Research; ST=Ship Track or Shipping Lane.

would lead to lower supersaturations and additional condensation. This warm phase mechanism is distinct from the cold phase mechanism outlined by Rosenfeld et al. (2008).

Invigoration of deep convection has been suggested by observations (e.g., Andreae, 2004; Khain, Cohen, et al., 2008; Koren et al., 2005), though some studies show that the aerosol signal and meteorology may not be independent in some cases (Nishant & Sherwood, 2017; Varble, 2018). Cloud-resolving simulations with and without artificial increases in aerosol concentrations (e.g., Fan et al., 2013; Khain et al., 2005; Khain, Cohen, et al., 2008) have also found signals suggestive of convective invigoration. However, long-term simulations of deep convection in radiative-convective equilibrium show only a short-lived response to a uniform increase in aerosol concentrations (Grabowski & Morrison, 2011) or to artificially enhanced latent heating and cooling that mimics the effects of increased cloud liquid in the mixed-phase region (Morrison & Grabowski, 2013). Sustained invigoration was found in simulations where latent heating and cooling were artificially amplified only in a localized region (Morrison & Grabowski, 2013).

Recently, Thornton et al. (2017) found significant increases in lightning above a well-trafficked shipping lane in the Indian Ocean that stretches from the southern tip of Sri Lanka to the northern tip of Sumatra (Figure 1a). As the lightning anomalies were not associated with similar anomalies in CAPE or precipitation, the aerosols produced by ships and their impact on microphysical processes in convective clouds were identified as the likely cause of the lightning increase over the shipping lane. (Note that all acronyms, including CAPE, are defined in a table at the end of the paper.)

Here the effects of the shipping lane on deep convection are modeled in an idealized setting to understand aerosol-induced changes in clouds and precipitation and their dynamical and radiative impact. While electrification is not simulated explicitly, some metrics useful as lightning proxies are explored. Rather than imposing anomalous latent heating as in Morrison and Grabowski (2013), any anomalous latent heating in these simulations arises from microphysical changes induced by aerosols emitted at the ocean surface.

2. Simulation Setup and Observational Data

Cloud-resolving simulations of radiative-convective equilibrium are performed over a spatially uniform sea surface temperature of 29 °C using the System for Atmospheric Modeling (Khairoutdinov & Randall, 2003), version 6.9. The simulations are run in a three-dimensional domain with $L_x = L_y = 384$ km, horizontal grid spacing of 1 km, and a domain top at 30 km. The vertical grid spacing is 250 m from 3- to 14-km altitude with finer resolution near the surface and coarser aloft. The simulation design is similar to the radiative-convective equilibrium simulations of Bretherton et al. (2005) except as described below. Cloud microphysics is treated using the double-moment microphysics of Morrison et al. (2005, 2009), radiative fluxes and heating are computed using RRTMG (Mlawer et al., 1997), and scalar advection follows Blossey and Durran (2008). Saturation adjustment is used in liquid clouds, which may underestimate convective invigoration by ~10–20% in terms

of convective mass flux and precipitation when compared to models that predict supersaturation (Lebo et al., 2012). The use of saturation adjustment also prevents the exploration of the warm-phase invigoration mechanism (Fan et al., 2018). The QuickBeam cloud radar simulator (Haynes et al., 2007) is used to compare the simulated cloud and precipitation fields to those that would be observed by the 13.8-GHz TRMM precipitation radar (TRMM PR., Iguchi et al., 2000). The simulated reflectivities are averaged onto a 4-km square grid to approximate the TRMM PR footprint of 5 km and set to zero where less than 17 dBZ, the TRMM minimum detectable echo.

The Morrison microphysics predicts cloud droplet number concentration and activates droplets from two modes of aerosol using the scheme of Abdul-Razzak and Ghan (2000). We specify a small, constant-in-time number concentration of coarse mode aerosol ($d = 1.3\mu$m, $\sigma_g = 2.5, N = 1.8\,\text{cm}^{-3}$), but the bulk of the aerosol available for activation is accumulation mode aerosol ($d = 0.052\mu$m, $\sigma_g = 2.04$) whose number mixing ratio (N_a) is advected and diffused like other prognostic scalar fields. An additional surface source of accumulation mode aerosol approximates the shipping lane, with uniform emission in time and along the shipping lane but localized in the cross-shipping-lane direction with a Gaussian profile of half width 12.5 km, following the pattern of emissions over the Indian Ocean shipping lane in the EDGAR ship emissions database (Crippa et al., 2016). (See Figure 1b.) A nascent mass of $1.5 \cdot 10^{-18}$ kg per aerosol particle is used to convert the EDGAR-derived mass emissions into number emissions, with the assumption that these aerosols would grow hygroscopically to accumulation mode size in the boundary layer. Aerosol removal by precipitation/cloud scavenging and coagulation is crudely represented by everywhere relaxing N_a toward a fixed, background value of 10^8 particles per kilogram of air on a time scale of 6 hr. The ratio of emissions rate to relaxation time scale fixes the size of the aerosol perturbation in the planetary boundary layer (PBL) over the shipping lane which drives microphysical changes in the clouds above. The microphysical setup resembles that in Berner et al. (2013), except for the simplified treatment of aerosol processing and the inclusion of ice microphysics.

To minimized transients at the start of the simulation, the initial profile was taken from the last 30 days of a 100-day-long small-domain simulation ($L_x = L_y$ =36 km). Nevertheless, substantial natural variability in the convection remains. Since aerosol-driven signals in important fields like precipitation and cloud radiative effects take tens of days to become statistically significant, the control simulation is run for 60 days to clearly discern them. A second, 30-day-long simulation was run with a fourfold increase in emissions (henceforth, 4×) to understand how the changes scale with aerosol concentration.

Except for the surface flux of accumulation mode aerosol, the model setup and forcings are homogeneous in the horizontal directions. Even without inhomogeneities in the forcings, such simulations can self-aggregate into dry and moist patches within the simulation domain as described by Bretherton et al. (2005). The beginning stage of self-aggregation occurs late in these simulations. To ensure that the results are not affected by this, the last 5 days of each simulation is excluded from the analysis.

3. Results and Discussion

The imposed surface flux of accumulation mode aerosol, which simulates the effect of shipping emissions, leads to an enhancement of N_a within the boundary layer above the shipping lane but only weak increases in the average concentration away from the shipping lane and above the PBL (Figure 2a). The enhanced N_a leads to increased in-cloud cloud droplet number mixing ratio, N_c, over the shipping lane, not only at cloud base but also throughout the lower troposphere (Figure 2b). Here N_c is sampled only where the cloud liquid mass mixing ratio $q_c > 10^{-6}$ kg kg^{-1}. As a result, the mean cloud droplet size is systematically decreased above the shipping lane (Figure 2c). Figure 2d shows that the surface aerosol flux doubles N_a at 0.5 km and in-cloud N_c at 1.2 km in the center of the shipping lane.

As suggested by Rosenfeld et al. (2008), smaller, more numerous cloud droplets at lower levels lead to an enhancement in cloud liquid water q_c at low levels above the shipping lane (Figure 3a), but the largest increase is higher in altitude, just above the 0 °C isotherm ($z = 4.4$ km). The increases in graupel mass mixing ratio q_g are larger than those in cloud liquid (Figure 3b). The increases in large hydrometeors above the shipping lane also affect the simulated radar reflectivity (Figure 3c) conditionally averaged over rainy columns with echo exceeding 20 dBZ below 1 km. These increases in reflectivity are broadly similar to those seen by the TRMM PR above the Indian Ocean shipping lane (Thornton et al., 2017; Figure 4a), though the area of enhanced reflectivity is narrower in the cross-shipping-lane direction and stronger increases in reflectivity are seen aloft.

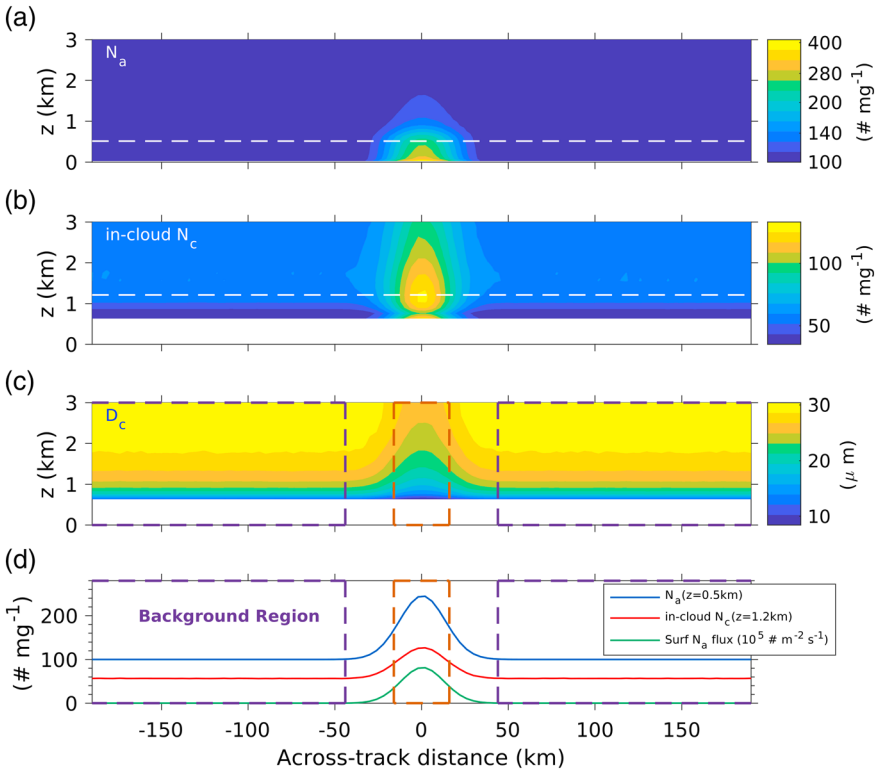

Figure 2. Time and along-shipping-lane averages of (a) accumulation mode aerosol number mixing ratio N_a, (b) in-cloud cloud droplet number mixing ratio N_c, (c) cloud liquid droplet volume mean diameter D_c, and (d) simulated shipping lane emissions along with N_a(z~500 m) and in-cloud N_c(z~1,200 m). The purple- and brown-dashed lines show the extent of the background region and shipping lane, respectively. The curves of N_a and in-cloud N_c in (d) are taken from the heights indicated by the white dashed lines in (a) and (b). The fields have been coarsened to 4 km in the horizontal before plotting. Time averages are over days 2–55.

In the simulations, hydrometeor increases above the shipping lane are supported by anomalous upward motion in the upper troposphere that peaks at approximately 10 km (Figure 3d). This upward motion occurs above the melting layer and is similar in magnitude to the mesoscale ascent seen in Figure 9 of Morrison and Grabowski (2013) in response to their enhanced latent heating and cooling.

3.1. Convective Invigoration

The differences between the shipping lane and background regions (brown and purple boxes in Figures 2 and 3) are further illustrated in Figure 4, which shows key time- and space-averaged profiles over the two regions. While N_a more than doubles within the PBL over the shipping lane, it returns to background levels quickly above the PBL top (Figure 4a). Despite this, in-cloud N_c is enhanced throughout the column, suggesting that convective updrafts locally carry the effects of larger N_a upward into the free troposphere. Increases in cloud liquid are most pronounced near the melting layer, but graupel increases throughout the mid and upper troposphere (Figure 4b).

As the invigoration hypothesis predicts, the apparent convective heating, Q_1, due to the combined effect of latent and radiative heating and convective-scale motions (Yanai & Johnson, 1993) also increases over the shipping lane above the melting layer (Figure 4c). This Q_1 increase across the shipping lane drives the upper tropospheric ascent seen in Figure 3d; it is mainly induced by enhanced convection rather than radiative heating. As the storage and horizontal advection terms are negligibly small, Q_1 is approximated by the shipping-lane- and background-region-mean vertical advection of liquid-ice static energy.

Time averages of various quantities related to the microphysics, dynamics, and radiative impacts of the aerosols are shown in Table 1 for both the background region and the change between the background region and the shipping lane for both the control and 4× (fourfold increase in emissions) simulations. As indicated by the standard errors, almost all of these differences are statistically significant at the 95% level.

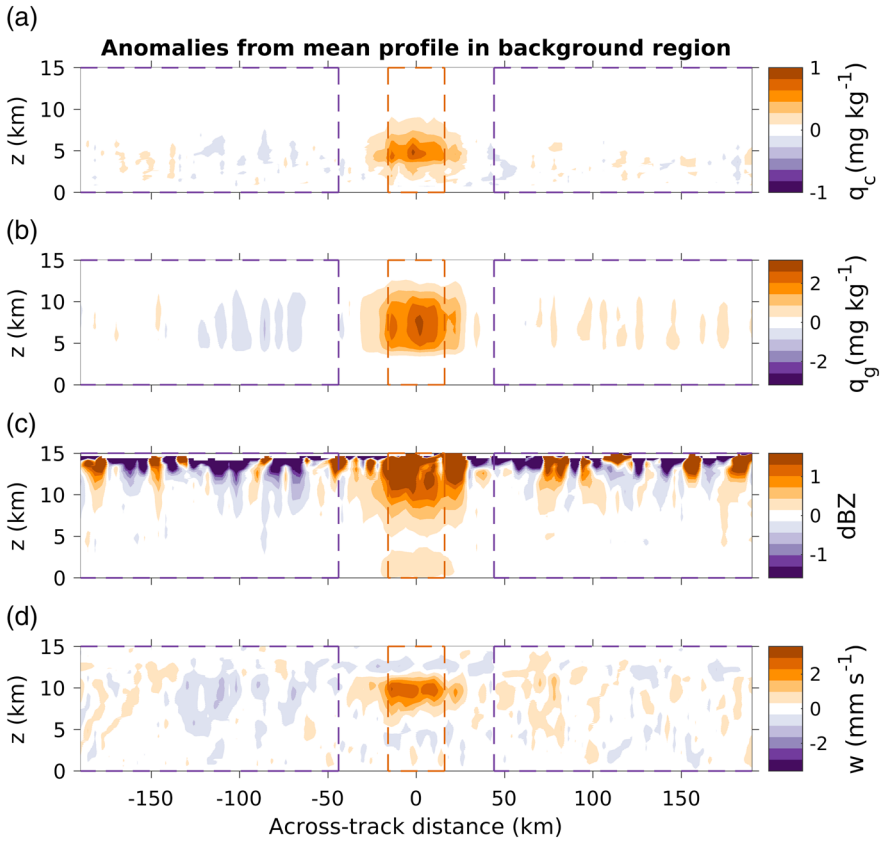

Figure 3. As in Figures 2a–2c, except that the anomaly of the time and zonal average from that in the background region is shown for (a) q_c, (b) q_g, (c) simulated radar reflectivity in rainy columns, and (d) vertical velocity, w. Blank areas at the top of (c) indicate regions without any reflectivities above 17 dBZ.

The invigoration of convection leads to increased precipitation at the surface in the shipping lane (Table 1), but the fractional increase in precipitation (~5%) is smaller than that in cloud cover (~10%) or in the vertically integrated amount of cloud liquid (~10%) and graupel (~25%). This suggests that the intensity of precipitation (precipitation amount per cloudy column) is lower in the shipping lane despite the overall increase in precipitation there, which (while defined differently) is consistent with the finding of Khain, BenMoshe, et al. (2008) that increased aerosols can reduce precipitation efficiency in deep convection. The modeled precipitation increase over the shipping lane is smaller than the ~6% standard error for TRMM PR-derived rain rate over the shipping lane, so that we cannot judge the realism of the modeled precipitation enhancement using these observations.

3.2. Enhancement of Intense Convection

Does the aerosol-induced convective invigoration documented in section 3.1 imply substantial changes in lightning like those observed over the Indian Ocean shipping lane by Thornton et al. (2017)? As the electric field associated with deep convective clouds and lightning discharges is not explicitly represented in our simulations, we seek lightning proxies calculable from our model variables. These include strong updrafts in the mixed-phase region (Barthe et al., 2010; Zipser & Lutz, 1994), liquid water and graupel amounts in the mixed-phase region (e.g., McCaul et al., 2009; Yair et al., 2010), and the abundance of cold echo tops (ETs) with strong radar reflectivities (Liu et al., 2012). While such indicators do not always perform well from storm to storm (Barthe et al., 2010), we expect them to have some statistical value. We wish to explain why the observed lightning frequency doubles over the Indian Ocean shipping lane given the comparatively modest relative increases in cloud and precipitation documented in section 3.1.

Strong updrafts (here $w > 10$ m/s) in region between 0 and −20 °C are thought to be necessary as a precursor to lightning (Zipser & Lutz, 1994). In our simulations (Figure 4d), the frequency of strong updrafts over the shipping lane is about about 10% larger than over the background region, which is no larger than the cloud

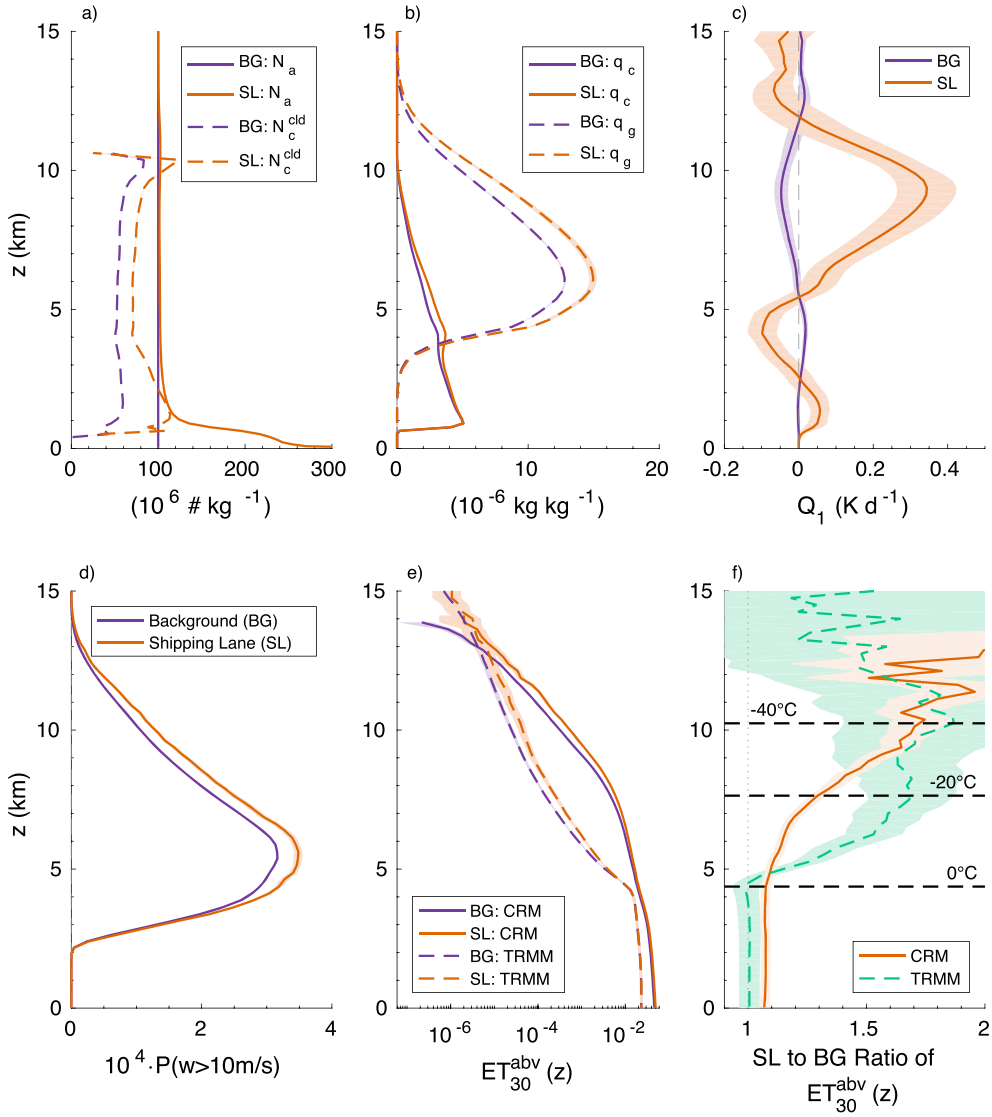

Figure 4. Time averaged vertical profiles for both the background region and shipping lane of (a) N_a and in-cloud N_c, (b) q_c and q_g, (c) apparent convective heating Q_1, (d) area fraction of strong updrafts ($w > 10$ m/s) at each level, and (e) the simulated area fraction with 30-dBZ echo tops above each height, z. (f) shows the shipping-lane-to-background-region ratio of the results in (e). (e) and (f) include results from TRMM over the Indian Ocean shipping lane. Light shading shows one standard error of the mean, computed separately for each level, around the sample mean. Where the shading is not visible, the standard error is comparable to or smaller than the width of the line. TRMM = Tropical Rainfall Measurement Mission; ET = echo top; CRM=Cloud Resolving Model.

fraction increase. Graupel and snow increase by 20–25% over the shipping lane (Figure 3b and Table 1), which is substantial but by itself not enough to explain the enhanced lightning.

In their analysis of lightning production by radar precipitation features (contiguous patches of echo detected by the TRMM PR), Liu et al. (2012) found a correlation between lightning and the presence of strong (>30 dBZ), cold echoes in a precipitation feature, with an ~50% chance of lightning for an oceanic precipitation feature whose 30-dBZ ET was colder than −40°C. Figure 4e shows profiles of ET_{30}^{abv}, the area fraction with a 30-dBZ echo above a given height z, for the background region and shipping lane in observations from TRMM and in the control simulation. For TRMM, the shipping lane is defined as 5.9 ± 0.2°N and the background region as 0.8–5 and 6.8–11°N. Above the melting level, ET_{30}^{abv} falls off more abruptly in TRMM, and the model overestimates ET_{30}^{abv} by a factor of ten or more. This error reflects the tendency for cloud-resolving models to produce excessive amounts of large ice hydrometeors in convective clouds (e.g., Stanford et al., 2017).

Table 1
Time- and Spatially Averaged Values of Various Quantities in the Background Region (BG) and the Difference Between Shipping Lane and Background Region (Δ) Are Shown Along With the Standard Error of the Difference SE_Δ for the Control Simulation and Another With a Fourfold Increase in the Surface Aerosol Flux (4×)

Variable	Units	BG	$\Delta \pm SE_\Delta$	$BG^{4\times}$	$\Delta^{4\times} \pm SE_\Delta^{4\times}$
N_a at $z = 0.5$ km	10^6 kg $^{-1}$	100.0197	117.0 ± 0.3	100.0287	463 ± 2
In-cloud N_c at $z = 1.2$ km	10^6 kg^{-1}	56.55	57.3 ± 0.3	56.52	202.4 ± 0.6
Surface precipitation	mm/day	2.75	0.16 ± 0.06	2.72	0.40 ± 0.11
Column cloud fraction	%	30.6	4 ± 1.6	29.5	11 ± 2
Vertical velocity at $z = 10$ km	mm/s	−0.3	2.5 ± 0.6	−1.0	6.9 ± 0.9
Cloud water path	g/m^2	17.38	1.9 ± 0.2	17.23	5.1 ± 0.5
Ice water path	g/m^2	11.8	2.4 ± 0.6	11.2	6.0 ± 1.0
Graupel water path	g/m^2	39.5	8 ± 1	38.3	21 ± 2
10-m/s updraft frac. ($T = -10$ °C)	10^{-4}	3.06	0.33 ± 0.07	2.97	0.88 ± 0.13
$ET^{abv}_{30dBZ}(z = 10$ km)	10^{-4}	2.73	1.9 ± 0.3	2.4	5.5 ± 0.9
Shortwave CRE at TOA	W/m^2	−31.5	-4.2 ± 1.2	−30.6	-11 ± 2
Longwave CRE at TOA	W/m^2	32.3	3.5 ± 1.5	31.5	9 ± 2
Net CRE at TOA	W/m^2	0.8	-0.7 ± 0.4	0.86	-1.8 ± 0.5
R_{clr} at TOA	W/m^2	117.14	0.43 ± 0.15	116.93	1.4 ± 0.3
R at TOA	W/m^2	117.9	-0.3 ± 0.4	117.8	-0.4 ± 0.4
R at surface	W/m^2	200.6	-3.8 ± 1.0	201.3	-10 ± 2
Implied ocean heating	W/m^2	114.3	-4.24 ± 1.1	115.2	-10 ± 2
Latent heat flux	W/m^2	80.28	0.34 ± 0.08	80.18	0.80 ± 0.13

Note. The final digit in each BG value is of the same magnitude as its standard error. The shipping lane is defined as the region less than 16 km from the location of peak emission, and the BG by $N_a < 1.01 \cdot 10^8$ kg^{-1} at 0.5 km. All differences are statistically significant at the 95% level except those in italics. CRE = cloud radiative effect; TOA = top of atmosphere.

While the absolute value of ET^{abv}_{30} is biased in the model, ET^{abv}_{30} is larger over the shipping lane than the background region in both TRMM and the model. Figure 4f shows the shipping-lane-to-background-region ratio of ET^{abv}_{30}, along with the standard error of the difference between the two regions divided by the background mean. The enhancement over the shipping lane grows stronger with height in both TRMM and the model, with similar values at 10 km (approximately −40 °C). TRMM's shipping-lane-to-background-region ratio of ET^{abv}_{30} at 10 km is 1.8 ± 0.4, which shows a marginally significant enhancement at the 95% confidence level and is comparable to the approximate doubling of observed lightning (Thornton et al., 2017). This suggests that ET^{abv}_{30} for $T = -40$ °C—here computed locally rather than for radar precipitation features—may be a reasonable proxy for lightning as foreseen by Liu et al. (2012).

3.3. Radiative Impacts

Koren et al. (2010) suggest that anthropogenic aerosol affects climate in part through changes to the radiative properties of deep convective clouds. (See also Rosenfeld et al., 2014.) This motivates looking for perturbations to the top-of-atmosphere (TOA) radiative fluxes above the shipping lane, with the caveats that the radiative response to a localized aerosol perturbation may differ from that to a broadly distributed anthropogenic aerosol increase and that our simulations do not include strong shear aloft that was seen as key to the spreading of cirrus clouds by Koren et al. (2010). The largest contributor to this radiative response is the net cloud radiative effect (CRE) at TOA (Table 1). In the background regions, the simulated net CRE is close to zero, consistent with observations of deep convective regions of the tropics (Ramanathan et al., 1989). Simulated changes in the magnitude of longwave and shortwave CRE over the shipping lane in our simulations are strong and statistically significant (~3–4 W/m^2). However, they partly cancel, and—when combined with the changes in clear-sky radiation—the total net downward radiative flux R at TOA is statistically indistinguishable between the shipping lane and background region. One could interpret the simulated changes in CRE within the shipping lane as due to increased cloud cover without a change in the CRE characteristic of a cloudy column. However, this result may be sensitive to the choice of microphysical scheme in the model.

The cancellation of longwave and shortwave effects does not hold at the surface, where decreased downwelling shortwave radiation above the shipping lane causes the net downward radiative flux at the surface to weaken ($\Delta R_{surf} = -3.6 \pm 0.9\,W/m^2$; Table 1). This implies a smaller net heat input into the oceanic-mixed layer. A simulation with interactive surface temperatures might experience slight surface cooling in the shipping lane, possibly weakening deep convection there.

4. Discussion and Conclusions

Aerosol-induced convective invigoration (Rosenfeld et al., 2008) has been found in 60-day cloud-resolving simulations under constant meteorological forcing (i.e., radiative convective equilibrium). As suggested by Morrison and Grabowski (2013), the simulated invigoration relies on localized aerosol perturbations that induce localized microphysical changes that are reinforced by weak mesoscale uplift above the shipping lane. While the simulated precipitation increase cannot be verified by TRMM observations above the Indian Ocean shipping lane that inspired this study, increased frequency of strong radar echoes aloft—a proxy for lightning—does correspond to lightning enhancement seen in Thornton et al. (2017). As our simulations do not permit supersaturation with respect to liquid, we have not been able to evaluate the recently proposed warm phase invigoration mechanism of Fan et al. (2018).

As seen in Table 1, the background-to-shipping-lane changes in microphysical, dynamical, and some radiative quantities increase by a factor of 2.5–3 from the control to 4× simulations. These are roughly proportional to the change in aerosol concentration: $N_a^{SL} \sim 2N_a^{BG}$ in the control simulation and $N_a^{SL} \sim 5N_a^{BG}$ in the 4× simulation. This suggests that the aerosol concentration itself may influence these changes.

Further features of the simulations—especially the changes in cloud radiative effects—may be sought in observations of the shipping lane and similar regions elsewhere: other shipping lanes, coastal cities in the tropics, or regions affected by planned reductions in shipping emissions (Sofiev et al., 2018). Constraining the aerosol perturbation in the boundary layer may be difficult due to extensive high cloud and the hydroscopic growth of aerosols near clouds (e.g., Chand et al., 2012). However, the robust signals in the simulations with a modest aerosol perturbation $N_a^{SL} \sim 2N_a^{BG}$ suggest that such signals may be detectable.

Acronyms

CAPE Convectively available potential energy
CRE Cloud radiative effect
CRM Cloud Resolving Model
EDGAR Emissions Database for Global Atmospheric Research
GCM General circulation model (or global climate model)
PBL Planetary boundary layer
RRTMG Rapid radiative transfer model for GCM applications
ST Ship Track or Shipping Lane
TOA Top of atmosphere
TRMM Tropical Rainfall Measurement Mission
WWLLN Worldwide Lightning Location Network

Acknowledgments
The authors would like to thank the two anonymous reviewers for their constructive comments. This work was supported by DOE awards DE-SC0011602 (P. B./C. B.) and DE-SC0018221 (J. T.), NOAA grant NA13OAR4310104 (P. B./C. B.), NSF award OISE-1743753 (P. B.), and the NASA Postdoctoral Program (K. V.). The EDGAR data are available from http://edgar.jrc.ec.europa.eu/overview.php?v=431. Other data and analysis scripts necessary to generate the figures and table are available at http://hdl.handle.net/1773/41969.

References

Abdul-Razzak, H., & Ghan, S. J. (2000). A parameterization of aerosol activation: 2. Multiple aerosol types. *Journal of Geophysical Research*, *105*(D5), 6837–6844. https://doi.org/10.1029/1999JD901161

Andreae, M. O. (2004). Smoking rain clouds over the Amazon. *Science*, *303*(5662), 1337–1342. https://doi.org/10.1126/science.1092779

Barthe, C., Deierling, W., & Barth, M. C. (2010). Estimation of total lightning from various storm parameters: A cloud-resolving model study. *Journal of Geophysical Research*, *115*, D24202. https://doi.org/10.1029/2010JD014405

Berner, A. H., Bretherton, C. S., Wood, R., & Muhlbauer, A. (2013). Marine boundary layer cloud regimes and POC formation in a CRM coupled to a bulk aerosol scheme. *Atmospheric Chemistry and Physics*, *13*, 12,549–12,572. https://doi.org/10.5194/acp-13-12549-2013

Blossey, P. N., & Durran, D. R. (2008). Selective monotonicity preservation in scalar advection. *Journal of Computational Physics*, *227*, 5160–5183. https://doi.org/10.1016/j.jcp.2008.01.043

Boucher, O., Randall, D., Artaxo, P., Bretherton, C., Feingold, G., Forster, P., et al. (2013). Clouds and aerosols. In T. F. Stocker, et al. (Eds.), *Climate change 2013: The physical science basis. Contribution of Working Group I to the Fifth Assessment Report of the Intergovernmental Panel on Climate Change* (pp. 571–657). Cambridge, United Kingdom and New York: Cambridge University Press.

Bretherton, C. S., Blossey, P. N., & Khairoutdinov, M. (2005). An energy-balance analysis of deep convective self-aggregation above uniform SST. *Journal of the Atmospheric Sciences*, *62*, 4273–4292. https://doi.org/10.1175/JAS3614.1

Chand, D., Wood, R., Ghan, S. J., Wang, M., Ovchinnikov, M., Rasch, P. J., et al. (2012). Aerosol optical depth increase in partly cloudy conditions. *Journal of Geophysical Research*, *117*, D17207. https://doi.org/10.1029/2012JD017894

Crippa, M., Janssens-Maenhout, G., Dentener, F., Guizzardi, D., Sindelarova, K., Muntean, M., et al. (2016). Forty years of improvements in European air quality: Regional policy-industry interactions with global impacts. *Atmospheric Chemistry and Physics*, *16*, 3825–3841. https://doi.org/10.5194/acp-16-3825-2016

Fan, J., Leung, L. R., Rosenfeld, D., Chen, Q., Li, Z., Zhang, J., & Yan, H. (2013). Microphysical effects determine macrophysical response for aerosol impacts on deep convective clouds. *Proceedings of the National Academy of Sciences of the United States of America*, *110*(48), E4581–E4590. https://doi.org/10.1073/pnas.1316830110

Fan, J., Rosenfeld, D., Zhang, Y., Giangrande, S. E., Li, Z., Machado, L. A. T., et al. (2018). Substantial convection and precipitation enhancements by ultrafine aerosol particles. *Science*, *359*(6374), 411–418. https://doi.org/10.1126/science.aan8461

Grabowski, W. W., & Morrison, H. (2011). Indirect impact of atmospheric aerosols in idealized simulations of convective–radiative quasi equilibrium. Part II: Double-moment microphysics. *Journal of Climate*, *24*, 1897–1912. https://doi.org/10.1175/2010JCLI3647.1

Haynes, J. M., Luo, Z., Stephens, G. L., Marchand, R. T., & Bodas-Salcedo, A. (2007). A multipurpose radar simulation package: QuickBeam. *Bulletin of the American Meteorological Society*, *88*, 1723–1727. https://doi.org/10.1175/BAMS-88-11-1723

Iguchi, T., Kozu, T., Meneghini, R., Awaka, J., & Okamoto, K. (2000). Rain-profiling algorithm for the TRMM precipitation radar. *Journal of Applied Meteorology*, *39*(12), 2038–2052. https://doi.org/10.1175/1520-0450(2001)040<2038:RPAFTT>2.0.CO;2

Khain, A. P., BenMoshe, N., & Pokrovsky, A. (2008). Factors determining the impact of aerosols on surface precipitation from clouds: An attempt at classification. *Journal of the Atmospheric Sciences*, *65*, 1721–1748. https://doi.org/10.1175/2007JAS2515.1

Khain, A., Cohen, N., Lynn, B., & Pokrovsky, A. (2008). Possible aerosol effects on lightning activity and structure of hurricanes. *Journal of the Atmospheric Sciences*, *65*, 3652–3677. https://doi.org/10.1175/2008JAS2678.1

Khain, A., Rosenfeld, D., & Pokrovsky, A. (2005). Aerosol impact on the dynamics and microphysics of deep convective clouds. *Quarterly Journal of the Royal Meteorological Society*, *131*, 2639–2663.

Khairoutdinov, M. F., & Randall, D. A. (2003). Cloud resolving modeling of the ARM summer 1997 IOP: Model formulation, results, uncertainties, and sensitivities. *Journal of the Atmospheric Sciences*, *60*, 607–625. https://doi.org/10.1175/1520-0469(2003)060<0607:CRMOTA>2.0.CO;2

Koren, I., Kaufman, Y. J., Rosenfeld, D., Remer, L. A., & Rudich, Y. (2005). Aerosol invigoration and restructuring of Atlantic convective clouds. *Geophysical Research Letters*, *32*, L14828. https://doi.org/10.1029/2005GL023187

Koren, I., Remer, L. A., Altaratz, O., Martins, J. V., & Davidi, A. (2010). Aerosol-induced changes of convective cloud anvils produce strong climate warming. *Atmospheric Chemistry and Physics*, *10*, 5001–5010. https://doi.org/10.5194/acp-10-5001-2010

Lebo, Z. J., Morrison, H., & Seinfeld, J. H. (2012). Are simulated aerosol-induced effects on deep convective clouds strongly dependent on saturation adjustment?*Atmospheric Chemistry and Physics*, *12*, 9941–9964. https://doi.org/10.5194/acp-12-9941-2012

Liu, C., Cecil, D. J., Zipser, E. J., Kronfeld, K., & Robertson, R. (2012). Relationships between lightning flash rates and radar reflectivity vertical structures in thunderstorms over the tropics and subtropics. *Journal of Geophysical Research*, *117*, D06212. https://doi.org/10.1029/2011JD017123

McCaul, E. W., Goodman, S. J., LaCasse, K. M., & Cecil, D. J. (2009). Forecasting lightning threat using cloud-resolving model simulations. *Weather Forecast*, *24*, 709–729. https://doi.org/10.1175/2008WAF2222152.1

Mlawer, E. J., Taubman, S. J., Brown, P. D., Iacono, M. J., & Clough, S. A. (1997). Radiative transfer for inhomogeneous atmospheres: RRTM, a validated correlated-k model for the longwave. *Journal of Geophysical Research*, *102*(D14), 16,663–16,682. https://doi.org/10.1029/97JD00237

Morrison, H., Curry, J. A., & Khvorostyanov, V. I. (2005). A new double-moment microphysics parameterization for application in cloud and climate models. Part I description. *Journal of the Atmospheric Sciences*, *62*, 1665–1677.

Morrison, H., & Grabowski, W. W. (2013). Response of tropical deep convection to localized heating perturbations: Implications for aerosol-induced convective invigoration. *Journal of the Atmospheric Sciences*, *70*, 3533–3555. https://doi.org/10.1175/JAS-D-13-027.1

Morrison, H., Thompson, G., & Tatarskii, V. (2009). Impact of cloud microphysics on the development of trailing stratiform precipitation in a simulated squall line: Comparison of one- and two-moment schemes. *Monthly Weather Review*, *137*, 991–1007. https://doi.org/10.1175/2008mwr2556.1

Nishant, N., & Sherwood, S. (2017). *A cloud-resolving model study of aerosol-cloud correlation in a pristine maritime environment*. https://doi.org/10.1002/2017GL073267

Ramanathan, V., Cess, R. D., Harrison, E. F., Minnis, P., Barkstrom, B. R., Ahmad, E., & Hartmann, D. (1989). Cloud-radiative forcing and climate: Results from the Earth Radiation Budget Experiment. *Science*, *243*(4887), 57–63. https://doi.org/10.1126/science.243.4887.57

Rosenfeld, D., Lohmann, U., Raga, G. B., O'Dowd, C. D., Kulmala, M., Fuzzi, S., et al. (2008). Flood or drought: How do aerosols affect precipitation? *Science*, *321*(5894), 1309–1313. https://doi.org/10.1126/science.1160606

Rosenfeld, D., Sherwood, S., Wood, R., & Donner, L. (2014). Climate effects of aerosol-cloud interactions. *Science*, *343*(6169), 379–380. https://doi.org/10.1126/science.1247490

Sofiev, M., Winebrake, J. J., Johansson, L., Carr, E. W., Prank, M., Soares, J., et al. (2018). Cleaner fuels for ships provide public health benefits with climate tradeoffs. *Nature Communications*, *9*(406). https://doi.org/10.1038/s41467-017-02774-9

Stanford, M. W., Varble, A., Zipser, E., Strapp, J. W., Leroy, D., Schwarzenboeck, A., et al. (2017). A ubiquitous ice size bias in simulations of tropical deep convection. *Atmospheric Chemistry and Physics*, *17*, 9599–9621. https://doi.org/10.5194/acp-17-9599-2017

Tao, W.-K., Chen, J.-P., Li, Z., Wang, C., & Zhang, C. (2012). Impact of aerosols on convective clouds and precipitation. *Reviews of Geophysics*, *50*, RG2001. https://doi.org/10.1029/2011RG000369

Thornton, J. A., Virts, K. S., Holzworth, R. H., & Mitchell, T. P. (2017). Lightning enhancement over major oceanic shipping lanes. *Geophysical Research Letters*, *44*, 9102–9111. https://doi.org/10.1002/2017GL074982

Varble, A. (2018). Erroneous attribution of deep convective invigoration to aerosol concentration. *Journal of the Atmospheric Sciences*, *75*(4), 1351–1368. https://doi.org/10.1175/JAS-D-17-0217.1

Yair, Y., Lynn, B., Price, C., Kotroni, V., Lagouvardos, K., Morin, E., et al. (2010). Predicting the potential for lightning activity in Mediterranean storms based on the Weather Research and Forecasting (WRF) model dynamic and microphysical fields. *Journal of Geophysical Research*, *115*, D04205. https://doi.org/10.1029/2008JD010868

Yanai, M., & Johnson, R. H. (1993). Impacts of cumulus convection on thermodynamic fields. In K. A. Emanuel & D. J. Raymond (Eds.), *The representation of cumulus convection in numerical models* (pp. 39–62). Boston, MA: American Meteorological Society.

Zipser, E. J., & Lutz, K. R. (1994). The vertical profile of radar reflectivity of convective cells: A strong indicator of storm intensity and lightning probability?*Monthly Weather Review*, *122*, 1751–1759. https://doi.org/10.1175/1520-0493(1994)122<1751:TVPORR>2.0.CO;2